https://doi.org/10.5194/acp-2020-817
Preprint. Discussion started: 25 August 2020

Atmospheric Chemistry and Physics Discussions
Open Access
EGU

Organized Variations in MBL Cloud Microphysical Properties Observed by Aircraft and Satellite and Simulated by Model

Dale M. Ward[1], Xiquan Dong[1]*, Baike Xi[1], Peng Wu[1], Xiaojian Zheng[1] and Yuan Wang[2,3]

1. Department of Hydrology and Atmospheric Sciences, University of Arizona, Tucson, AZ, 85710
2. Division of Geological and Planetary Sciences, California Institute of Technology, Pasadena,15 CA 91125, USA
3. Jet Propulsion Laboratory, California Institute of Technology, Pasadena, CA

Submitted to ACP Special Issue: Marine aerosols, trace gases, and clouds over the north Atlantic, August 3, 2020

**Corresponding author address*: Dr. Xiquan Dong, The Department of Hydrology and Atmospheric Sciences, University of Arizona, 1133 E. James Rogers Way, PO Box 210011, Tucson, AZ 85721-0011, USA. Email: xdong@email.arizona.edu; Phone: 520-621-4652.

https://doi.org/10.5194/acp-2020-817
Preprint. Discussion started: 25 August 2020

Atmospheric Chemistry and Physics Discussions

Abstract

Marine boundary layer (MBL) clouds in subtropical regions strongly impact global energy balance, but complete understanding of the processes that control their microphysical properties remain elusive. We analyze aircraft in-situ measurements of MBL clouds for two selected cases from the ACE-ENA field campaign that contain mesoscale convective cells (MCCs) on the order of tens of kilometers embedded in the large-scale overcast cloud field. The aircraft flight tracks aligned with the MCC organization, such that vertically-stacked, horizontal flight legs alternated between sampling clouds along organized MCCs and sampling clouds between MCCs. This alignment is well-suited to study the distinctly different microphysical properties for the two cloud regimes. Clouds within organized MCCs had lower droplet concentrations, but larger droplet sizes and liquid water contents with enhanced drizzle relative to clouds between MCCs. While observed aerosol properties below these two cloud regimes are generally consistent with their corresponding cloud microphysical properties, preexisting organization of the aerosol field was probably not required in the development of the MCC organization. In contrast, the lower aerosol and CCN concentrations observed below the MCC cloud layer most likely developed from precipitation and coalescence scavenging. A cloud-resolving WRF model simulation with realistic large-scale forcing reproduces the MCC organization of the cloud field suggesting that updraft velocity is the key to explain the differences in cloud microphysics. Both observations and model simulations indicate that under moderate-heavy drizzling conditions, precipitation and coalescence scavenging dominates and drives spatial gradients of cloud droplets, aerosols and CCN concentrations rather than local sources.

https://doi.org/10.5194/acp-2020-817
Preprint. Discussion started: 25 August 2020

Atmospheric Chemistry and Physics Discussions

1. Introduction

Owing to their substantial role in the Earth's radiation budget, and consequently, their effect on the Earth's climate, low-level stratiform clouds have been a topic of considerable interest since the publication of the classic paper describing their physics (Lilly, 1968). Marine boundary layer (MBL) clouds in subtropical regions strongly influence the regional and global climate system (e.g., Klein and Hartmann, 1993). Over the ocean, MBL clouds are common with a strong temperature inversion at the top of the MBL, which provides conditions favorable for MBL cloud formation (Lilly, 1968). These MBL clouds are maintained by vertical mixing, which is primarily due to the strong longwave radiative cooling at the cloud top generating turbulence to provide an upward moisture flux from the ocean surface (Albrecht et al., 1995; Rémillard et al., 2012; Wood, 2012; Wood et al., 2015).

The climatic importance of the MBL cloud microphysical and macrophysical properties, particularly the cloud fraction (CF), cloud-droplet effective radius (r_e), number concentration (N_c), and liquid water content/path (*LWC/LWP*), is widely recognized. Climate models disagree substantially in the magnitude of cloud feedback for the regimes of subtropical MBL clouds (Bony et al. 2005 and 2006, Lohmann et al. 2005), and suffer from the so-called 'too few, too bright' problem (Allan et al., 2007, Nam et al., 2012, Webb et al., 2013, IPCC 2013). The 'too few' problem, an underestimate in cloud amount, allows more solar radiation to reach the surface. The 'too bright' problem, an overestimate in cloud albedo due to an overestimate in the amount of liquid water within the cloud, causes more sunlight to be reflected. It is therefore imperative to have more accurate MBL cloud properties through long-term ground-based observations, as well as aircraft in situ measurements, so that we can improve their representation in climate models.

Aerosol-cloud-precipitation interactions are a significant source of uncertainty for MBL clouds (e.g., Wood, 2012). Aerosol generation resulting from natural and anthropogenic activities is expected to have considerable, far-reaching effects on cloud development and the hydrological cycle. Though the aerosol direct effect can simply be thought of as a reduction of incoming solar radiation reaching the Earth surface, the aerosol indirect effect (AIE) involves a complex set of aerosol-cloud-precipitation interactions. AIEs include the alteration of cloud properties such as cloud lifetime, droplet size distribution, liquid water content and path (*LWC, LWP*), cloud optical depth (COD), and albedo (Penner et al., 2004; Dong et al., 2005, 2006, 2014; Ghan et al., 2016).

https://doi.org/10.5194/acp-2020-817
Preprint. Discussion started: 25 August 2020

Several studies indicate that MBL clouds under the regions of relatively higher sub-cloud aerosol concentrations have reduced r_e, increased N_c, and enhanced *LWC/LWP* and COD than clouds under clean regions (Twohy et al., 2005; Lu et al., 2007; Dong et al., 2015). However, recent observational studies, e.g., Toll et al. (2017), indicate that the *LWP* response to increased aerosol concentrations is bidirectional and depends upon a host of different meteorological parameters.

The Eastern North Atlantic (ENA) is a region of persistent subtropical MBL clouds (Dong et al., 2014). The region is commonly covered by large swaths of stratocumulus cloud sheets. The stratocumuli commonly form to the east of the position of the subtropical ridge in a region of large-scale subsidence. Synoptic scale variability in low cloud cover has been associated with changes in the strength and position of the subtropical high (Wood, 2012). Even within synoptic regions with fully overcast low-level stratocumulus cloud decks, small scale organized mesoscale convective cells (MCCs) can develop (Miller et al. 1995). The Aerosol and Cloud Experiments in the Eastern North Atlantic (ACE-ENA) field campaign was conducted during two intensive observation periods (IOPs): early summer 2017 (June 21 to July 20) and winter 2018 (January 11 to February 20) (Wang et al., 2019; Wu et al., 2020). The DOE Atmospheric Radiation Measurement (ARM) Aerial Facility (AAF) Gulfstream-159 (G-1) research aircraft flew from Terceira Island in the Azores during IOPs. There were 20 flights during the summer 2017 IOP and 19 flights during the winter 2018 IOP. There are approximately 158 total hours with aircraft in-situ measurements during ACE-ENA IOP (Wang et al., 2019; Wu et al., 2020).

Two cases, July 18, 2017 and January 25, 2018, were selected during the ACE-ENA for this study. The aircraft in-situ measurements and satellite observations for the selected two cases reveal that there are significant, organized MCCs over an area of about 600 km^2. The aircraft flight patterns were L shaped with one leg aligned with the cloud-level wind direction and the other leg across the cloud-level winds. In this study, we focus on these two cases in which aircraft sampled two distinct cloud regimes due to the alignment of the flight path with the mesoscale organization of the cloud field. In both cases, a portion of the flight path aligned with an organized band or MCC with enhanced drizzle, while the other portion of the flight path mostly crossed different organized bands or MCCs with light drizzle. The terms along-wind and cross-wind are used throughout this paper to distinguish the two different spatial regions sampled over the entire flight path. These

https://doi.org/10.5194/acp-2020-817
Preprint. Discussion started: 25 August 2020

names are not meant to imply a causal link between the wind or flight direction and the observed differences in cloud microphysical properties.

In this study, we explore the large differences in cloud microphysical properties for two distinct cloud regimes embedded within large-scale overcast stratocumulus clouds. We further investigate the causes for the different MBL cloud microphysical properties for the July 18 case using a cloud-resolving WRF (CR-WRF) model simulation with realistic large-scale forcing. Section 2 specifies the in-situ aircraft data, satellite data, reanalysis meteorological data, and the CR-WRF model run used in this study. Results are shown in section 3 followed by a brief summary and discussion in section 4.

2. Data and Model

The aircraft data used in this study come from the ACE-ENA field campaign collected on July 18, 2017 and January 25, 2018. Cloud and drizzle microphysical properties are derived from measurements made by the Fast Cloud Droplet Probe (FCDP) and the 2-Dimensional Stereo (2DS-V) probe at 1 Hz. Microphysical parameters are computed each second using observations of droplet size distributions (DSDs) over a range of particle size bins. Aircraft position is provided by the Aircraft-Integrated Meteorological Measurement System (AIMMS-20).

Cloud microphysical properties are computed from FCDP observations of droplet concentrations in 18 discrete size bins, which include droplets with diameters ranging from 1.5 to 46 µm. Drizzle microphysical properties are computed from 2DS-V observations of droplet concentrations in 40 size bins, which includes drops with diameters ranging from 45 to 975 µm. An observation is considered to contain cloud if the cloud droplet number concentration (N_c) is greater than 5 cm^{-3} and drizzle if the drizzle droplet number concentration (N_d) is greater than 0.01 cm^{-3}. Only observations verified to contain cloud or drizzle are included in the results presented. The cloud condensation nuclei (CCN) concentrations below cloud base and above cloud top measured by the Dual-Column CCN Counter were used to determine the number concentration of activated CCN at two supersaturation levels (S=0.15% and S=0.35%) at 1 Hz. In this study, the CCN concentrations (N_{CCN}) at S=0.15% are used. The aerosol concentration below the cloud layer was observed by the Passive Cavity Aerosol Spectrometer (PCASP). The PCASP has 30 size bins, which include particle diameters ranging from 100 to 3200 nm. We used the PCASP observed aerosol concentrations rather than the Fast Integrated Mobility Spectrometer (FIMS) and the

https://doi.org/10.5194/acp-2020-817
Preprint. Discussion started: 25 August 2020

Atmospheric Chemistry and Physics Discussions

Condensation Particle Counter (CPC) because the data have fewer spikes, its size range spanning the accumulation size mode is a good proxy for condensation nuclei, and it is an external probe, which alleviates concerns about processing time delay.

In addition to aircraft in-situ measurements, concurrent satellite observations and retrievals are used in this study in order to investigate the spatiotemporal variations of MBL cloud properties. The MBL cloud optical depth τ and cloud-droplet effective radius r_e retrieved from the Meteosat-9 satellite operated by the European Organization for the Exploitation of Meteorological Satellites (EUMETSAT) were used to look for patterns in the large-scale horizontal MBL cloud structures (Minnis et al., 2011). The large-scale meteorological conditions are obtained from the ERA5 reanalysis.

The Weather Research and Forecast (WRF) model version 3.6 is employed in this study to simulate the case on July 18, 2017. Four nested domains are used with a horizontal resolution of 19.2 km, 4.8 km, 1.2 km, and 300 m, respectively. The innermost domain is configured as a quasi large-eddy simulation with the 3D Smagorinsky first-order closure for eddy coefficient computation. The 65 stretched sigma levels are used with a 40-m vertical resolution in PBL. The large-scale forcing is adopted from ERA5 reanalysis (25 km resolution). To accurately depict cloud microphysical processes in the MBL cloud, a spectral bin scheme is employed which utilizes 33 bins to represent cloud/rain drops and aerosols separately (Wang et al., 2013). The model integrates from 12:00 UTC, July 17 to 00:00 UTC, July 19 and the first half day is considered as spin-up. Shortwave and longwave radiation transfer calculations are accounted for by the Goddard and RRTM schemes, respectively.

3. Results and Discussion

3.1 Cloud Results

Figure 1 shows the horizontal and vertical flight paths on July 18, 2017 and January 25, 2018 over the time that cloud data were collected for this study. In both cases, the aircraft flew at several nearly constant altitude paths (horizontal legs) spanning from near cloud base to near cloud top. The horizontal flight legs were vertically stacked, repeating L shaped patterns. In both cases, one arm of the L was closely aligned with the cloud-level wind direction and motion, while the other arm was across the cloud-level wind direction. Horizontal legs in the along-wind direction are

https://doi.org/10.5194/acp-2020-817
Preprint. Discussion started: 25 August 2020

depicted in blue, while horizontal legs in the cross-wind direction are red. Each of these horizontal segments contains about 270 one-second observations of the DSD and is about 25 km in length using a representative aircraft speed of 90 ms^{-1}. The designations along-wind and cross-wind are simply used to separate the data collected along each direction. These names are not meant to imply a causal link between the wind or flight direction and the observed differences in cloud microphysical properties. However, what initially caught our attention was the distinctly different cloud microphysical properties observed in the along-wind flight legs compared with the cross-wind flight legs in the July 18 case. We later identified January 25 as a similar case observed during the winter IOP. Before detailing the distinctly different cloud microphysical properties along each flight leg direction, we will briefly look at the large-scale synoptic patterns from these two days.

The synoptic patterns at cloud altitude are shown in Figure 2. On July 18, the observation area was in between a high-pressure system well to the west-southwest and a low-pressure system to the northeast. The prevailing wind at 900 hPa was northwesterly. On January 25, the center of the 850 hPa high was just a few hundred km southwest of the observation area, and the prevailing wind was north-northeasterly. The pressure gradient and hence cloud level winds are stronger in July. Mean wind speeds can be estimated from in-situ observations on the aircraft and the interpolated sounding at ENA site by averaging the wind speed over the cloud altitude range and observation time. The mean cloud-level wind speed on July 18 was 7.7 ms^{-1} from aircraft measurements and 7.5 ms^{-1} from the interpolated sounding. The mean cloud-level wind speed on January 25 was 2.9 ms^{-1} from aircraft and 0.84 ms^{-1} from the interpolated sounding. The wind arrows in Fig. 2 are fixed size and do not indicate wind speed.

Satellite retrievals of COD provide a large-scale view of cloud horizontal structures. Figure 3 shows the satellite-retrieved COD on July 18 at 10:00 and 10:30 UTC. Both images show bands with enhanced COD that roughly line up with the cloud-level wind direction (NW – SW). Between these bands, COD is reduced. Examination of the half-hourly satellite retrievals of COD over this region from 9:00 to 11:00 UTC indicates that the cloud field tended to organize into bands of higher COD that lined up along the prevailing winds. Between 10:00 and 10:30 UTC, as the aircraft was sampling the middle and upper portions of the clouds, a band of enhanced COD is aligned

https://doi.org/10.5194/acp-2020-817
Preprint. Discussion started: 25 August 2020

with the along-wind flight track, while the cross-wind flight track flew through several bands including their edges and centers with relatively large variations in COD.

Figure 4 shows the satellite retrieved COD on January 25 at 12:00 and 12:30 UTC. Again, there are horizontal structures in the retrieved COD, but it is difficult to make out a dominant pattern of banded structures as observed on July 18. Examination of the half-hourly satellite retrievals of COD over this region from 11:00 to 1:00 UTC indicates that areas of enhanced COD tend to move slowly along the prevailing northerly winds, though there is also dissipation and strengthening of cloud elements happening. Between 12:00 and 12:30 UTC, as the aircraft was sampling the middle and upper portions of the clouds, a region of enhanced COD covered much of the along-wind flight track, while most of the cross-wind flight track was covered by a region of much lower COD. This is consistent with the lower percentage of 1 Hz in-situ measurements in the cross-wind flight track that met the cloud identification criteria in the middle of the clouds depicted in Fig. 1d.

The vertical thermodynamic structures obtained from the ARM interpolated sounding product are shown in Figure 5. The atmosphere is well mixed below the cloud base with a strong temperature inversion and drying immediately above the cloud top on both days, which is common for this region. The lower atmosphere contains much more water vapor on July 18 with a lower cloud base (~600 m) compared to January 25 (~1300 m). The mean cloud thickness is slightly greater on July 18 (~400 m) compared to January 25 (~300 m).

Figures 6 and 7 show that there are large systematic differences in the aircraft in-situ measured cloud and drizzle microphysical properties between the along- and cross-wind legs on July 18 and January 25, respectively. Cloud microphysical properties are computed from each measurement of the FCDP droplet size distribution (DSD) from 1.5 to 46 µm. Mean cloud properties are computed by averaging all 1 Hz measurements that meet the cloud present criteria ($N_c > 5$ cm^{-3}) along each defined horizontal leg. Drizzle microphysical properties are computed from each measurement of the 2DS-V drop size distribution from 45 to 975 µm. Mean drizzle properties are computed by averaging all 1Hz measurements that meet the drizzle present criteria ($N_d > 0.01$ cm^{-3}) along each defined leg.

On July 18 (Figure 6), the mean cloud-droplet radius (r_c) and cloud liquid water content (LWC_c) increase with altitude on both the along- and cross-wind sides as expected, but their means at each leg altitude are quite different. Mean N_c is largest in the middle of the clouds and decreases toward

https://doi.org/10.5194/acp-2020-817
Preprint. Discussion started: 25 August 2020

Atmospheric Chemistry and Physics
Discussions

cloud top probably due impacts from cloud top entrainment and growth of cloud droplets to drizzle drops. The along-wind side has a larger mean r_c and LWC_c, but lower N_c than the cross-wind side at each leg altitude. The vertical distributions of drizzle drop radius, r_d, and number concentration, N_d, are opposite to their cloud counterparts with high concentrations of small drizzle drops near the cloud top and fewer, but larger drizzle drops near the cloud base. The highest N_d near the cloud top was converted from cloud droplets through the autoconversion process (Wood, 2005) and additional water vapor through the evaporation of smaller cloud droplets during cloud-top entrainment. These drizzle drops fall when the gravitational force exceeds the buoyancy force and grow further by collecting cloud droplets and small drizzle drops through the collision-coalescence process. As drizzle drops fall, accretion becomes increasingly important (Wood, 2005). Figure 6 also shows that more drizzle is being generated on the along-wind side as r_d, N_d, and LWC_d are generally larger at the same leg altitudes throughout the clouds. The mean vertical profiles of the drizzle microphysical properties within the cloud vary generally as expected for both legs. Specifically, r_d decreases but N_d and LWC_d increase with altitude.

Figure 7 from January 25 is similar to Fig. 6 in that the profiles of the mean cloud and drizzle microphysical properties vary generally as expected with altitude. It is also similar in that the along-wind side has a lower N_c, but larger r_c and LWC_c with more drizzle than the cross-wind side. One difference is that the N_c is much smaller in the middle of the cloud on January 25. This is consistent with lower aerosol and CCN concentrations and less water vapor below the cloud layer on January 25 as described later.

Figures 8 and 9 show the differences between the cloud microphysical properties computed each second from the along- and cross-wind measurements of the DSD in the middle portion of the clouds on July 18 and January 25. Restricting in-situ measurements to the mid-cloud horizontal legs reduces the impact of cloud edge effects. Figures 8a and 9a show the mean DSDs along horizontal flight legs at approximately 850 m and 1380 m in altitude, respectively. The mean cloud DSDs based on FCDP observations extend from 1.5 to 45 µm and the mean drizzle DSDs based on 2DS-V observations extend from 45 to 975 µm. In both cases, there are higher concentrations of smaller cloud droplets with diameters less than 20 to 25 µm observed on the cross-wind side, and higher concentrations of larger cloud droplets and drizzle drops on the along-wind side. Large

https://doi.org/10.5194/acp-2020-817
Preprint. Discussion started: 25 August 2020

cloud droplets (r_c~20 μm) on the along-wind side in both cases provide embryonic drizzle droplets that grow to drizzle-sized drops through the collision-coalescence process near the cloud top.

The scatterplots in Fig. 8 for July 18 show almost bi-modal type differences between the along- and cross-wind observations. Generally, the along-wind observations have relatively tighter clusters with smaller N_c, but larger r_c and LWC_c than the cross-wind observations. The scatterplots in Fig. 9 for January 25 have much more overlap between the along- and cross-wind observations. But there is a cluster of along-wind observations with relatively lower N_c, larger r_c and higher LWC_c where no cross-wind observations fall. The larger r_c and higher LWC_c along-wind sides on both days most likely result from stronger updrafts and low-level moisture convergence, which is more likely to lead to drizzle formation.Further investigation this point is carried out by running a WRF model simulation, which is included section 3.3. The next section discusses cloud-aerosol interactions using observed aerosol data.

3.2 Aerosol Discussion

A plausible explanation for some of the differences in cloud properties might be different aerosol concentrations in along- and cross-wind sides. For example, fewer available CCN in the along-wind direction could result in lower N_c and large r_c (Platnick and Twomey, 1994; Painemal et al., 2015). The mean aerosol concentrations in the along- and cross-wind legs are similar to their corresponding N_c values in the middle of the cloud layer (80 cm^{-3} and 120 cm^{-3}) as shown in Figure 6b, while the mean CCN concentrations are greater and lower, respectively, than their N_c values near the cloud base (40 cm^{-3} along and 65 cm^{-3} cross). This is possible since the CCN concentration was measured at 0.15% supersaturation. Using the 0.35% supersaturation observations (not shown), the mean CCN concentrations just below cloud base increase to just over 70 cm^{-3} in both the along- and cross-wind legs, which both are greater than N_c near the cloud base, but still lower than the N_c values in the middle of the cloud layer. Hudson and Noble (2013) report that effective cloud supersaturations often exceed 1% in stratus clouds that form in clean marine air, and thus both CCN measurements may be underestimates. We believe the aerosol concentrations measured by the PCASP instrument provide the best estimates of available CCN.

As shown in Figure 10, the mean observed aerosol and CCN concentrations are lower for the along-wind side relative to the cross-wind side for both (a) above ocean and (b) below cloud base legs. Specifically, the mean aerosol concentration measured just below cloud base on the along-

https://doi.org/10.5194/acp-2020-817
Preprint. Discussion started: 25 August 2020

wind side is 28% lower than on the cross-wind side. The lower aerosol and CCN concentrations on the along-wind side may be largely due to drizzle coalescence scavenging. Following the method of Wood (2006), the loss rate of CCN over then entire cloud-containing mixed layer due to drizzle scavenging can be estimated from the cloud base precipitation rate, the depth of the MBL, and the cloud thickness. We computed precipitation rates at cloud base at 1 Hz using the observed DSDs for the horizontal legs near cloud base. Mean precipitation rates of 6.4 mm day^{-1} (moderate to heavy drizzle) and 0.93 mm day^{-1} (modest drizzle) were obtained by averaging over the cloud base legs for the along- and cross-wind measurements, respectively. The corresponding CCN loss rates are -463 cm^{-3} day^{-1} (-19 cm^{-3} hr^{-1}) and -100 cm^{-3} day^{-1} (-4 cm^{-3} hr^{-1}). The greater along-wind CCN loss rate is consistent with the lower aerosol concentrations observed on the along-wind side. While there are many factors that determine aerosol/CCN concentration, the estimated differential scavenging rate (along-wind minus cross-wind) by itself could produce the observed differences in below cloud aerosol in ~1.5 h.

Figure 11 shows that the observed aerosol and CCN concentrations on January 25 are also lower on the along-wind leg, which has lower N_c and more drizzle, relative to the cross-wind leg, which higher has lower N_c and less drizzle. However, for this case the observed aerosol concentrations are lower than the middle cloud N_c and the observed CCN concentrations are lower than the cloud base N_c for both the along- and cross-wind legs. The observed aerosol concentration on the along-wind leg is 24% lower than on the cross-wind leg. Again, this difference may be largely due to drizzle coalescence scavenging. Mean precipitation rates at cloud base are 11.2 mm day^{-1} (moderate to heavy drizzle) and 0.33 mm day^{-1} (light drizzle) on the along- and cross-wind legs. The corresponding CCN loss rates are -277 cm^{-3} day^{-1} (-12 cm^{-3} hr^{-1}) and -10 cm^{-3} day^{-1} (-0.4 cm^{-3} hr^{-1}). Again, while there are many factors that determine aerosol/CCN concentration, the estimated differential scavenging rate by itself could produce the observed differences in above ocean aerosol in ~1 h.

Figure 12 also qualitatively supports the idea that the along- and cross-wind differences in below cloud aerosol are highly influenced by the differential rates of drizzle coalescence scavenging. In addition to having lower mean aerosol concentrations, the along-wind measurements have higher concentrations of large accumulation mode aerosols (diameter > 1.0 µm) and lower concentrations of small accumulation mode aerosols (diameter < 0.3 µm). The shift in aerosol size distribution is

https://doi.org/10.5194/acp-2020-817
Preprint. Discussion started: 25 August 2020

expected as evaporated drizzle drops leave behind larger aerosols that combine the CCN collected during the coalescence process. On July 18, this effect is more pronounced in the leg just below the cloud base relative to the leg just above the ocean. The shift to larger aerosols on January 25 observed just above the ocean is obvious, but even less pronounced. It would have been nice to have observations from a horizontal flight leg just below the cloud base on January 25.

3.3 WRF simulation

To further investigate different cloud microphysical properties in the along- and cross-wind legs, we employed a nested CR-WRF simulation with a spectral bin microphysics scheme to simulate the evolution of the cloud field on July 18. The model run starts from 12:00 UTC, July 17 to 00:00 UTC, July 19 and the first half day is considered as model spin-up. The model begins with the large-scale observed background aerosol, which is uniform across the inner domain. The model shows that the specific meteorological conditions present on July 18 are conducive for the formation of organized bands of enhanced drizzle that align with the wind direction. Figure 13a shows that the WRF simulation does produce the basic pattern of COD captured by the satellite retrievals in Figure 3. Specifically, organized bands of higher COD line up with the wind direction without prescribing variation in the below cloud CCN.

Figure 13b shows the model generated vertical velocity at 848 m and 10:00 UTC. The banded regions of enhanced COD in the model are associated with narrow bands of enhanced upward vertical velocity. While the largest COD values coincide with the narrow band of upward vertical velocity, the band of enhanced COD extends laterally outward, indicating that drizzle formation extends laterally away from the updraft core. The organized structure of the mesoscale convective cells embedded in the overcast stratus cloud deck on July 18, 2017 was captured by both the satellite observations and model simulations. Substantial drizzle is often associated with cellular convection in stratocumulus layers (Albrecht et al., 1995; Miller et al., 1995). The stronger updraft core that coincided with the along-wind flight path enhances the activation of CCN (Hudson and Noble, 2013) which increases LWC_c. The enhanced updraft also lifts more large cloud droplets into the upper part of the cloud layer where cloud droplets start to convert into drizzle drops by the autoconversion process. Drizzle-size drops that form near the top of the cloud, then start to fall and grow by collecting cloud droplets and smaller drizzle drops through the accretion process, which further reduces N_c and N_d.

https://doi.org/10.5194/acp-2020-817
Preprint. Discussion started: 25 August 2020

The drizzle growth processes of collision and coalescence effectively combine the CCN within the many collected droplets into a single, larger CCN that is left behind when drizzle drops evaporate after falling below the cloud base. In regions of active drizzle, this recycling of CCN through the cloud results in the reduction in the total CCN concentration (mainly loss of smaller CCN), but an increase in large CCN below cloud base. In both cases studied, clouds that were observed to be producing more drizzle (the along-wind flight segments) were associated with fewer, but larger CCN below the cloud base relative to the clouds that were producing less drizzle (the cross-wind flight segments).

4. Summary and Conclusions

Aircraft in-situ measurements obtained on July 18, 2017 and January 25, 2018 during the ACE-ENA IOP reveal two distinct cloud regimes on each day within overcast MBL clouds. Specifically, the aircraft flight patterns consisted of horizontal legs at several altitudes below and through the cloud layers that alternated between along-wind flight paths sampling clouds within organized regions of enhanced convection and drizzle and cross-wind flight paths mostly sampling clouds through several MCCs or enhanced bands which include the edges and centers of MCCs. This alignment of the flight track and mesoscale cloud organization is well suited to study the distinctly different cloud microphysical properties for the two cloud regimes. The designations along-wind and cross-wind are simply used to distinguish the two spatial regions sampled. By chance the mesoscale cloud structures of enhanced convection fell within the along-track portions of the flight paths on these two days. We did not find evidence for a causal link between the wind or flight direction and the observed differences in cloud microphysical properties. The different cloud microphysical properties in the along- and cross-wind directions are primarily due to sampling different cloud regimes within the mesoscale pattern of cloud variation.

The aircraft in-situ measurements in the along-wind legs had smaller N_c, larger r_c and LWC_c, and more drizzle than those in the cross-wind legs. Based on the aircraft in situ measurements of cloud and aerosol properties, as well as satellite retrievals and a CR-WRF simulation, we conclude that the different MBL cloud microphysical properties in the along- and cross-wind flight observations are not due to variations in the background aerosol conditions. In other words, different aerosol and CCN concentrations below the cloud layer in the along- and cross-wind legs are not the causes of different cloud microphysical properties between two legs. In contrast, we did find that the

https://doi.org/10.5194/acp-2020-817
Preprint. Discussion started: 25 August 2020

lower aerosol and CCN concentrations below the cloud layer in the along-wind legs were modified by drizzle coalescence scavenging. Specifically, the along-wind legs had enhanced drizzle and large CCN loss rates but higher concentrations of large accumulate mode aerosols, relative to the cross-wind observations where less drizzle production was observed.

The large-scale cloud field for these cases is best represented as bi-modal cloud structures with organized mesoscale structures of enhanced convection and drizzle that form within an overcast MBL cloud field. Combining the along- and cross-wind observations and treating the cloud field as a homogenous MBL cloud would be misleading in these cases. Mean vertical profiles produced by combining the along- and cross-wind observations shown in Figures 6 and 7 would not be representative of the cloud microphysical properties observed in either the organized regions of enhanced convection or the regions falling between them. Similarly, scatterplots and mean DSDs that do not distinguish the underlying cloud organization would miss the distinctly different microphysical properties of the clouds within each regime. This bi-modal behavior is crucial to be considered for both model simulations and ground-truth evaluation of remote sensing retrievals.

The results from this study have important implications on studying aerosol-cloud-precipitation interactions using aircraft, surface, or satellite measurements. Even with similar aerosol background conditions and within the same dynamic regime, clouds may organize into regions or bands with distinctly different microphysical properties. Caution should be taken when analyzing aerosol indirect effect with fixed *LWP*/*LWC*, since the differences in cloud microphysics might result from the cloud structure variations rather than from aerosol effects.

https://doi.org/10.5194/acp-2020-817
Preprint. Discussion started: 25 August 2020

Acknowledgements

The aircraft and ground-based measurements were obtained from the Atmospheric Radiation Measurement (ARM) Program sponsored by the U.S. Department of Energy (DOE) Office of Energy Research, Office of Health and Environmental Research, and Environmental Sciences Division. The data can be downloaded from https://www.archive.arm.gov/discovery/#v/results/s/s::aceena. This study was primarily supported by the NSF project under grant AGS-1700728 at the University of Arizona and also supported as part of the "Enabling Aerosol - cloud interactions at Global convection - permitting scalES (EAGLES)" project (74358), funded by the U.S. Department of Energy, Office of Science, Office of Biological and Environmental Research, Earth System Modeling program with the subcontract to the University of Arizona. Dr. Dale Ward was partially supported by UA EDO seed grant. Special thanks to Dr. Jian Wang, PI of ACE-ENA and the team of scientists and technicians who made this work possible by maintaining the instruments and collecting and processing the aircraft data for the ACE-ENA field campaign. Dr. Yuan Wang acknowledges the funding support from NSF (Award No. 1700727) at Cal Tech. ERA5 atmospheric reanalysis of the global climate is provided by Copernicus Climate Change Service Climate Data Store (CDS) (https://cds.climate.copernicus.eu/cdsapp#!/home).

https://doi.org/10.5194/acp-2020-817
Preprint. Discussion started: 25 August 2020

References

Albrecht, B. A., Bretherton, C. S., Johnson, D., Schubert, W. H. and Frisch, A. S.: The Atlantic Stratocumulus Transition Experiment - ASTEX, Bull. - Am. Meteorol. Soc., doi:10.1175/1520-0477(1995)076<0889:TASTE>2.0.CO;2, 1995.

Allan, R. P., Slingo, A., Milton, S. F., and Brooks, M. E.: Evaluation of the Met Office global forecast model using Geostationary Earth Radiation Budget (GERB) data, Quart. J. Roy. Meteor. Soc., doi:10.1002.qj.166., 2007.

Bony, S. and Dufresne, J. L.: Marine boundary layer clouds at the heart of tropical cloud feedback uncertainties in climate models, Geophys. Res. Lett., doi:10.1029/2005GL023851, 2005.

Bony, S., Colman, R., Kattsov, V. M., Allan, R. P., Bretherton, C. S., Dufresne, J.-L., Hall, A., Hallegatte, S., Holland, M. M., Ingram, W., Randall, D. A., Soden, B. J., Tselioudis, G. and Webb, M. J.: How Well Do We Understand and Evaluate Climate Change Feedback Processes?, J. Clim., doi: 10.1175/JCLI3819.1., 2006.

Cess, R. D., Potter, G. L., Blanchet, J. P., Boer, G. J., Del Genio, A. D., Deque, M., Dymnikov, V., Galin, V., Gates, W. L., Ghan, S. J. and Kiehl, J. T.: Intercomparison and interpretation of climate feedback processes in 19 atmospheric general circulation models, J. Geophys. Res., doi: 10.1029/JD095iD10p16601, 1990.

Cess, R. D., Zhang, M. H., Ingram, W. J., Potter, G. L., Alekseev, V., Barker, H. W., Cohen-Solal, E., Colman, R. A., Dazlich, D. A., Del Genio, A. D. and Dix, M. R.: Cloud feedback in atmospheric general circulation models: An update, J. Geophys. Res., doi: 10.1029/96JD00822, 1996.

Dolinar, E. K., Dong, X., Xi, B., Jiang, J. H. and Su, H.: Evaluation of CMIP5 simulated clouds and TOA radiation budgets using NASA satellite observations, Clim. Dyn., doi:10.1007/s00382-014-2158-9, 2015.

Dong, X., Minnis, P. and Xi, B.: A climatology of midlatitude continental clouds from the ARM SGP central facility: Part I: Low-level cloud macrophysical, microphysical, and radiative properties, J. Clim., doi:10.1175/JCLI3342.1, 2005.

Dong, X., Xi, B. and Minnis, P.: A climatology of midlatitude continental clouds from the ARM SGP Central Facility. Part II: Cloud fraction and surface radiative forcing, J. Clim., doi:10.1175/JCLI3710.1, 2006.

Dong, X., Xi, B., Kennedy, A., Minnis, P. and Wood, R.: A 19-month record of marine aerosol–

https://doi.org/10.5194/acp-2020-817
Preprint. Discussion started: 25 August 2020

cloud–radiation properties derived from DOE arm mobile facility deployment at the azores. Part I: cloud fraction and single-layered MBL cloud properties, J. Clim., doi: 10.1175/JCLI-D-13-00553.1, 2014.

Dong, X., Schwantes, A. C., Xi, B. and Wu, P.: Investigation of the marine boundary layer cloud and CCN properties under coupled and decoupled conditions over the azores, J. Geophys. Res., doi:10.1002/2014JD022939, 2015.

Ghan, S., Wang, M., Zhang, S., Ferrachat, S., Gettelman, A., Griesfeller, J., Kipling, Z., Lohmann, U., Morrison, H., Neubauer, D. and Partridge, D. G.: Challenges in constraining anthropogenic aerosol effects on cloud radiative forcing using present-day spatiotemporal variability, Proc. Natl. Acad. Sci. U. S. A., doi: 10.1073/pnas.151403613, 2016

Hill, A. A., Feingold, G. and Jiang, H.: The influence of entrainment and mixing assumption on aerosol–cloud interactions in marine stratocumulus, J. Atmos. Sci., doi: 10.1175/2008JAS2909.1, 2009.

Hudson, J. G. and Noble, S.: CCN and vertical velocity influences on droplet concentrations and supersaturations in clean and polluted stratus clouds, J. Atmos. Sci., doi:10.1175/JAS-D-13-086.1, 2014.

IPCC, Climate Change 2013: The Physical Science Basis. Contribution of Working Group I to the Fifth Assessment Report of the Intergovernmental Panel on Climate Change [Stocker, T.F., D. Qin, G.-K. Plattner, M. Tignor, S.K. Allen, J. Boschung, A. Nauels, Y. Xia, V. Bex and P.M. Midgley (eds.)]. Cambridge University Press, Cambridge, United Kingdom and New York, NY, USA, 1535 pp, doi:10.1017/CBO9781107415324, 2013.

Klein, S. A., and Hartmann, D. L.: The seasonal cycle of stratiform clouds. J. Clim., doi: 10.1175/1520-0442(1993)006<1587:TSCOLS>2.0.CO;2., 1993.

Lamer, K., Puigdomènech Treserras, B., Zhu, Z., Isom, B., Bharadwaj, N. and Kollias, P.: Characterization of Shallow Oceanic Precipitation using Profiling and Scanning Radar Observations at the Eastern North Atlantic ARM Observatory, Atmos. Meas. Tech., doi: 10.5194/amt-12-4931-2019, 2019

Lilly, D. K.: Models of cloud-topped mixed layers under a strong inversion, Quart. J. Roy. Meteor, Soc., doi: 10.1002/qj.49709440106 ,1968.

Logan, T., Xi, B. and Dong, X.: Aerosol properties and their influences on marine boundary layer cloud condensation nuclei at the ARM mobile facility over the Azores, J. Geophys. Res.,

https://doi.org/10.5194/acp-2020-817
Preprint. Discussion started: 25 August 2020

Atmospheric Chemistry and Physics Discussions

doi:10.1002/2013JD021288, 2014.

Lu, M. L., Conant, W. C., Jonsson, H. H., Varutbangkul, V., Flagan, R. C. and Seinfeld, J. H.: The marine stratus/stratocumulus experiment (MASE): Aerosol-cloud relationships in marine stratocumulus, J. Geophys. Res., doi:10.1029/2006JD007985, 2007.

Lohmann, U. and Feichter, J: Global indirect aerosol effects: a review, Atmos. Chem. Phys., doi: 10.5194/acp-5-715-2005, 2005

Mann, J. A., Christine Chiu, J., Hogan, R. J., O'Connor, E. J., L'Ecuyer, T. S., Stein, T. H. and Jefferson, A.: Aerosol impacts on drizzle properties in warm clouds from ARM Mobile Facility maritime and continental deployments, J. Geophys. Res., doi:10.1002/2013JD021339, 2014.

Miller, M. A. and Albrecht, B. A.: Surface-based observations of mesoscale cumulus-stratocumulus interaction during ASTEX, J. Atmos. Sci., doi:10.1175/1520-0469(1995)052<2809:SBOOMC>2.0.CO;2, 1995.

Minnis, P., Sun-Mack, S., Young, D. F., Heck, P. W., Garber, D. P., Chen, Y., Spangenberg, D. A., Arduini, R. F., Trepte, Q. Z., Smith, W. L., Ayers, J. K., Gibson, S. C., Miller, W. F., Hong, G., Chakrapani, V., Takano, Y., Liou, K. N., Xie, Y. and Yang, P.: CERES edition-2 cloud property retrievals using TRMM VIRS and Terra and Aqua MODIS data-Part I: Algorithms, IEEE Trans. Geosci. Remote Sens., doi:10.1109/TGRS.2011.2144601, 2011.

Nam, C., Bony, S., Dufresne, J. L. and Chepfer, H.,: The 'too few, too bright'tropical low-cloud problem in CMIP5 models, Geophys. Res. Lett., doi:10.1029/2012GL053421, 2012.

Painemal, D., Minnis, P. and Nordeen, M.: Aerosol variability, synoptic-scale processes, and their link to the cloud microphysics over the northeast Pacific during MAGIC, J. Geophys. Res., doi: 10.1002/2015JD023175, 2015.

Penner, J. E., Dong, X. and Chen, Y.: Observational evidence of a change in radiative forcing due to the indirect aerosol effect, Nature, doi:10.1038/nature02234, 2004.

Platnick, S. and Twomey, S.: Determining the susceptibility of cloud albedo to changes in droplet concentration with the Advanced Very High Resolution Radiometer, J. Appl. Meteorol., doi:10.1175/1520-0450(1994)033<0334:dtsoca>2.0.co;2, 1994.

Rémillard, J., Kollias, P., Luke, E. and Wood, R.: Marine boundary layer cloud observations in the Azores, J. Clim., doi: 10.1175/JCLI-D-11-00610.1, 2012.

Soden, B. J., and Vecchi, G. A.: The vertical distribution of cloud feedback in coupled ocean-atmosphere models, Geophys. Res. Lett., doi: 10.1029/2011GL047632, 2011.

Toll, V., Christensen, M., Gasso, S., and Bellouin, N.: Volcano and ship tracks indicate excessive aerosol-induced cloud water increases in a climate model, Geophys. Res. Lett., doi:10.1002/2017GL075280, 2017.

Twohy, C. H., Petters, M. D., Snider, J. R., Stevens, B., Tahnk, W., Wetzel, M., Russell, L. and Burnet, F.: Evaluation of the aerosol indirect effect in marine stratocumulus clouds: Droplet number, size, liquid water path, and radiative impact, J. Geophys. Res. D Atmos., doi:10.1029/2004JD005116, 2005.

Wang, J., et al.: Aerosol and Cloud Experiments in Eastern North Atlantic (ACE-ENA) Field Campaign Report. Ed. by Robert Stafford, ARM user facility. DOE/SC-ARM-19-012. Available from https://www.osti.gov/biblio/1526025, 2019.

Wang, Y., Fan, J., Zhang, R., Leung, L. R. and Franklin, C.: Improving bulk microphysics parameterizations in simulations of aerosol effects, J. Geophys. Res. Atmos., doi:10.1002/jgrd.50432, 2013.

Webb, M. J., Lambert, F. H. and Gregory, J. M.: Origins of differences in climate sensitivity, forcing and feedback in climate models, Clim. Dyn., doi:10.1007/s00382-012-1336-x, 2013.

Wood, R.: Drizzle in stratiform boundary layer clouds: Part II: Micorphysical aspects. J. Atmos. Sci., doi:10.1175/JAS3530.1, 2005.

Wood, R.: Rate of loss of cloud droplets by coalescence in warm clouds, J. Geophys. Res. Atmos., doi:10.1029/2006JD007553, 2006.

Wood, R.: Stratocumulus clouds. Monthly Weather Review, doi:10.1175/MWR-D-11-00121.1, 2012.

Wood, R., Wyant, M., Bretherton, C. S., Rémillard, J., Kollias, P., Fletcher, J., Stemmler, J., De Szoeke, S., Yuter, S., Miller, M., Mechem, D., Tselioudis, G., Chiu, J. C., Mann, J. A. L., O'Connor, E. J., Hogan, R. J., Dong, X., Miller, M., Ghate, V., Jefferson, A., Min, Q., Minnis, P., Palikonda, R., Albrecht, B., Luke, E., Hannay, C. and Lin, Y.: Clouds, aerosols, and precipitation in the marine boundary layer: An arm mobile facility deployment, Bull. Am. Meteorol. Soc., doi:10.1175/BAMS-D-13-00180.1, 2015.

Wu, P., Dong, X., Xi, B., Tian, J. and Ward, D. M.: Profiles of MBL Cloud and Drizzle Microphysical Properties Retrieved From Ground-Based Observations and Validated by Aircraft In Situ Measurements Over the Azores, J. Geophys. Res. Atmos., doi:10.1029/2019JD032205, 2020.

https://doi.org/10.5194/acp-2020-817
Preprint. Discussion started: 25 August 2020

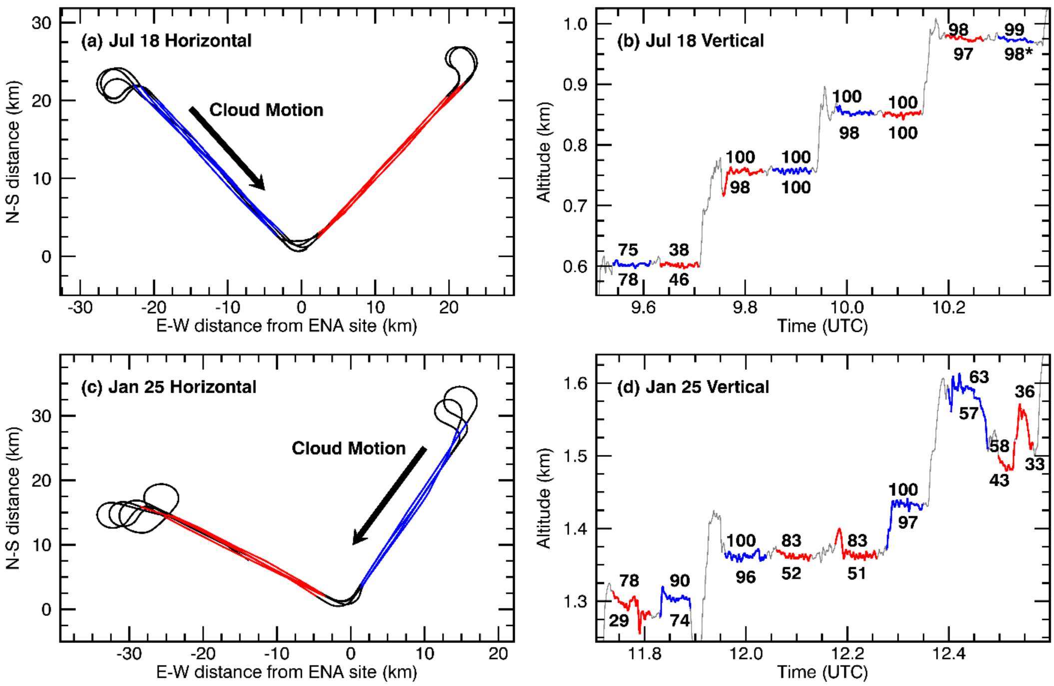

Figure 1. Horizontal and vertical flight paths for the periods of data collection on July 18 (a, b) and January 25 (c, d). Along-wind legs are blue and cross-wind legs are red. Horizontal distances are relative to the ARM radar facility at (39.09°N, 28.03°W). The numbers above and below the flight legs in the vertical plots are the percentage of observations along the leg that meet the criteria for cloud and drizzle, respectively (* denotes that over 80% of the 2DS-V observations were missing).

https://doi.org/10.5194/acp-2020-817
Preprint. Discussion started: 25 August 2020

Atmospheric Chemistry and Physics
Discussions

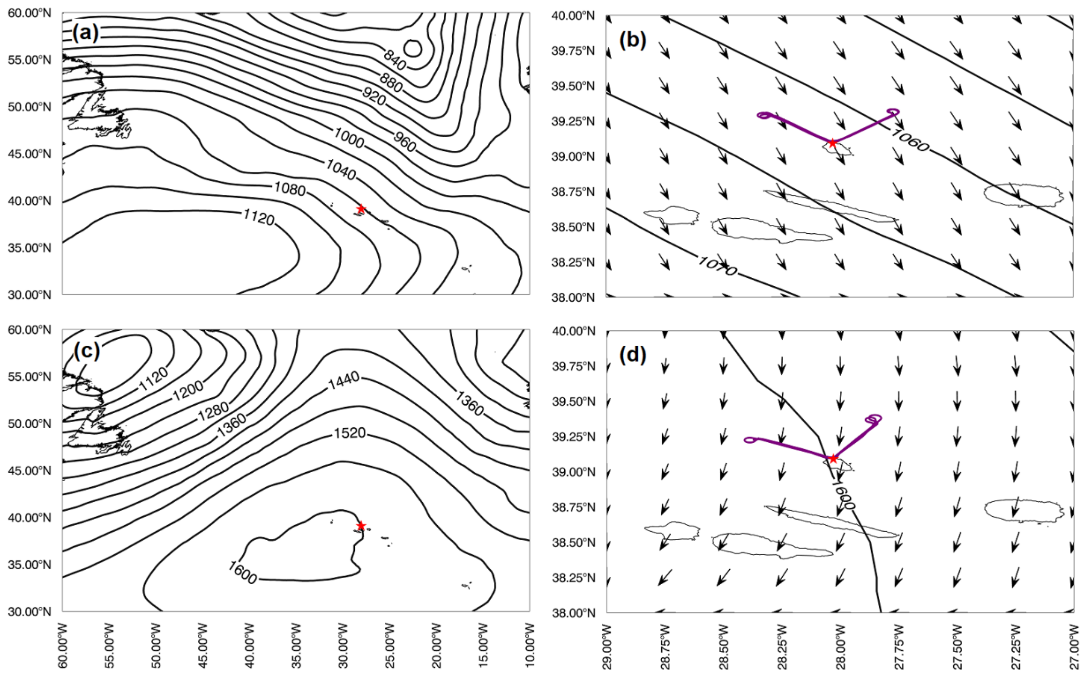

Figure 2. 900 hPa geopotential height from ERA5 on July 18, 2017 (a, b) and 850 hPa geopotential height on January 25, 2018 (c, d). The red star indicates the position ARM radar facility. Arrows in (b) and (d) represent the wind direction only within a grid box of 2° x 2°, not the wind speed. Purple lines show the horizontal flight track.

https://doi.org/10.5194/acp-2020-817
Preprint. Discussion started: 25 August 2020

Atmospheric Chemistry and Physics
Discussions

548

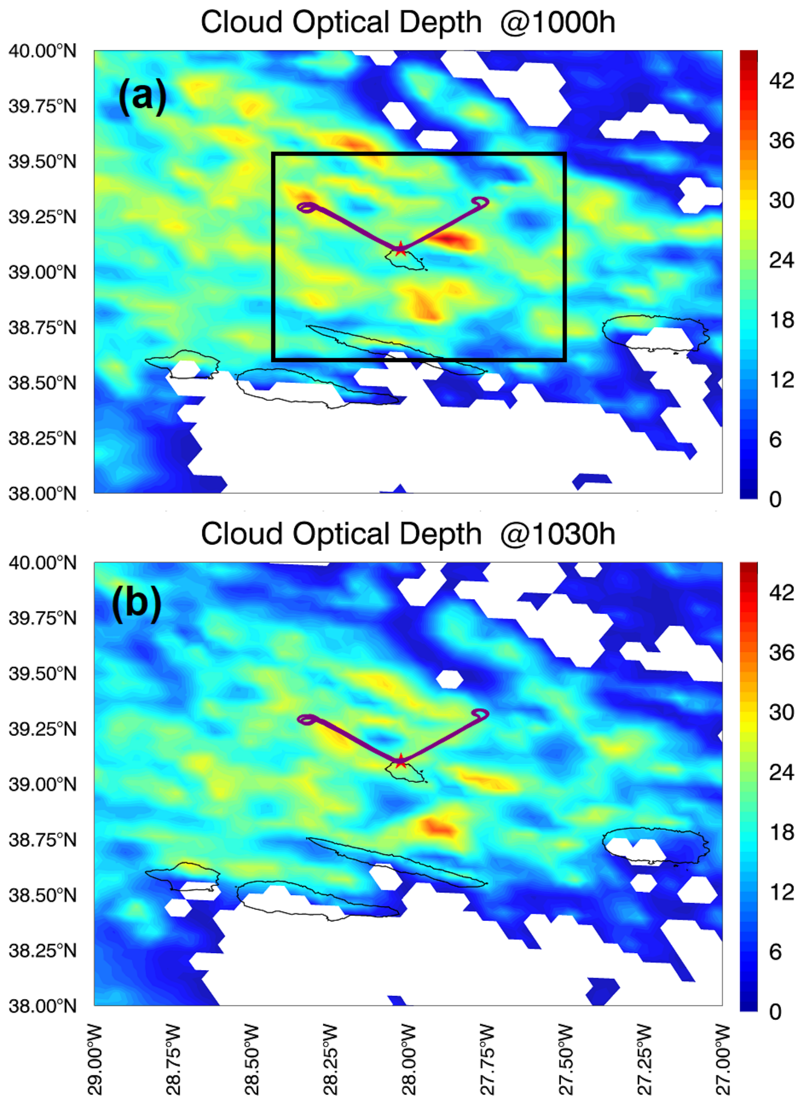

549

550

551 **Figure 3**. Meteosat images (4-km resolution) for cloud optical depth on July 18, 2017, at (a) 10
552 and (b) 10:30 UTC over a 2° by 2° box centered on the ARM radar facility marked with a star.
553 Horizontal flight track shown in purple. Region inside black box in (a) shows corresponding WRF
554 simulation inner domain shown in Fig. 13.

555

https://doi.org/10.5194/acp-2020-817
Preprint. Discussion started: 25 August 2020

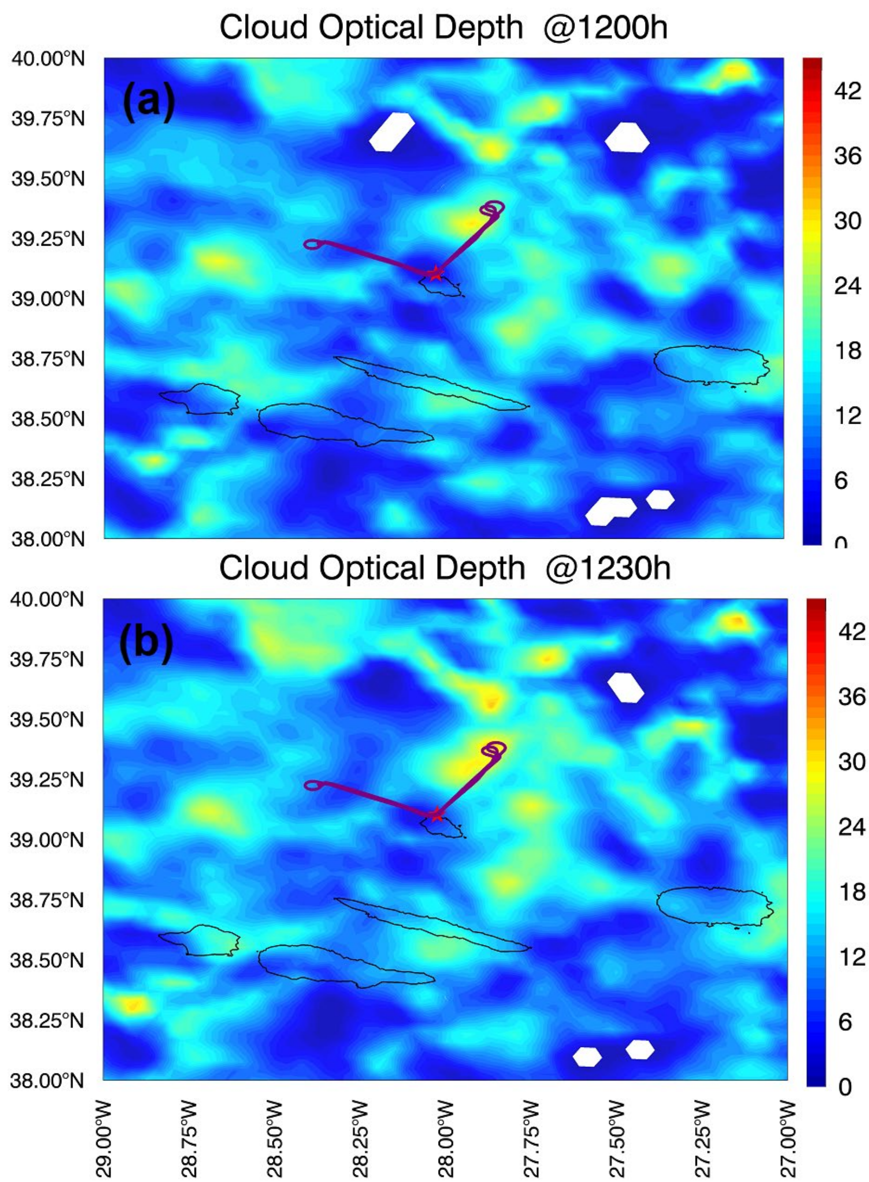

Figure 4. Meteosat images (4-km resolution) for cloud optical depth on January 25, 2018, at (a) 12:00 and (b) 12:30 UTC over a 2° by 2° box centered on the ARM radar facility marked with a star. Horizontal flight track shown in purple.

https://doi.org/10.5194/acp-2020-817
Preprint. Discussion started: 25 August 2020

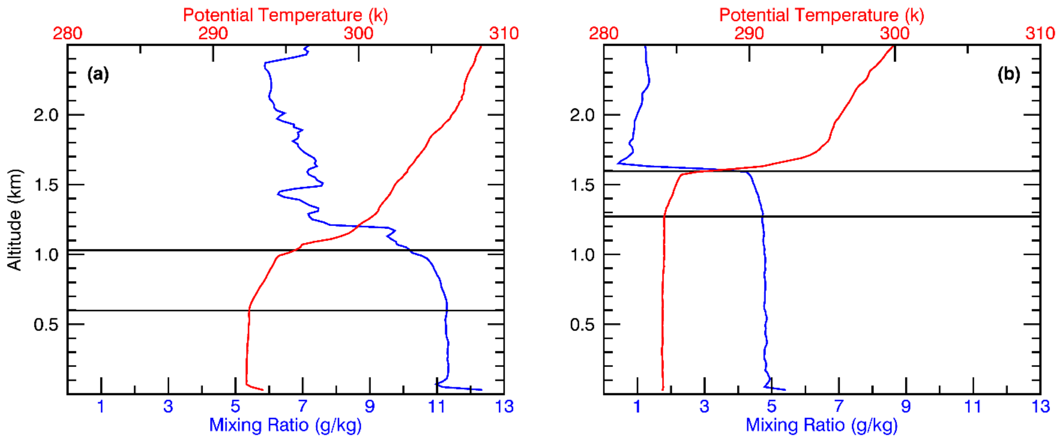

Figure 5. Profiles of potential temperature and mixing ratio on (a) July 18 and (b) January 25. Values obtained from the ARM interpolated sounding product. Horizontal black lines indicate the approximate altitudes of the cloud top and cloud base.

https://doi.org/10.5194/acp-2020-817
Preprint. Discussion started: 25 August 2020

Atmospheric Chemistry and Physics
Discussions

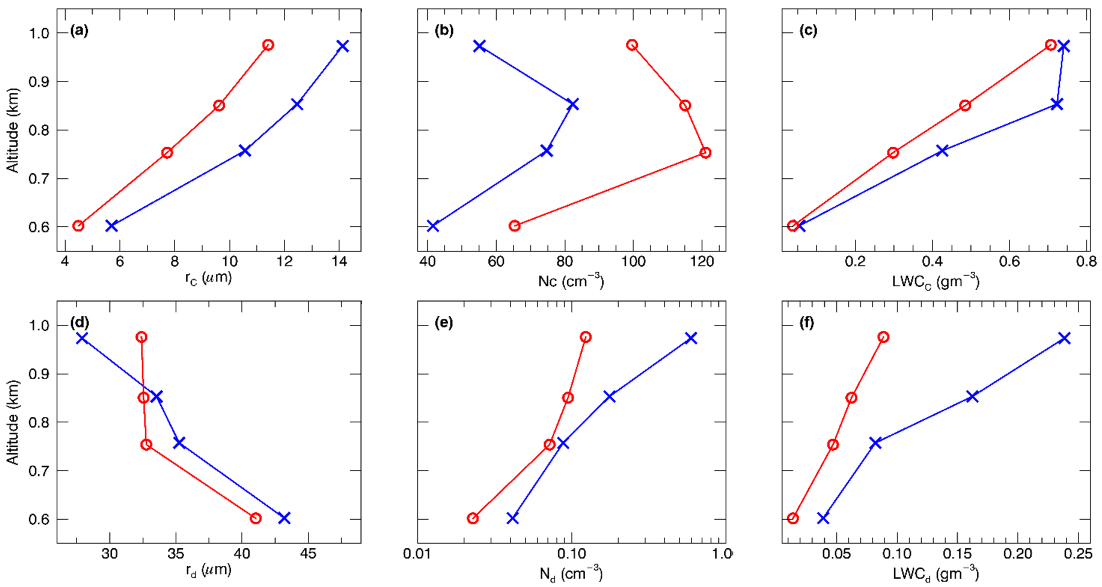

Figure 6. Mean values of various cloud and drizzle microphysical properties computed from the 1 Hz aircraft observations along the horizontal legs shown in Fig. 1b for July 18: (a) cloud droplet radius, (b) cloud droplet number concentration, (c) cloud droplet liquid water content, (d) drizzle v radius, (e) drizzle droplet number concentration, and (f) drizzle droplet liquid water content.

https://doi.org/10.5194/acp-2020-817
Preprint. Discussion started: 25 August 2020

Atmospheric Chemistry and Physics
Discussions

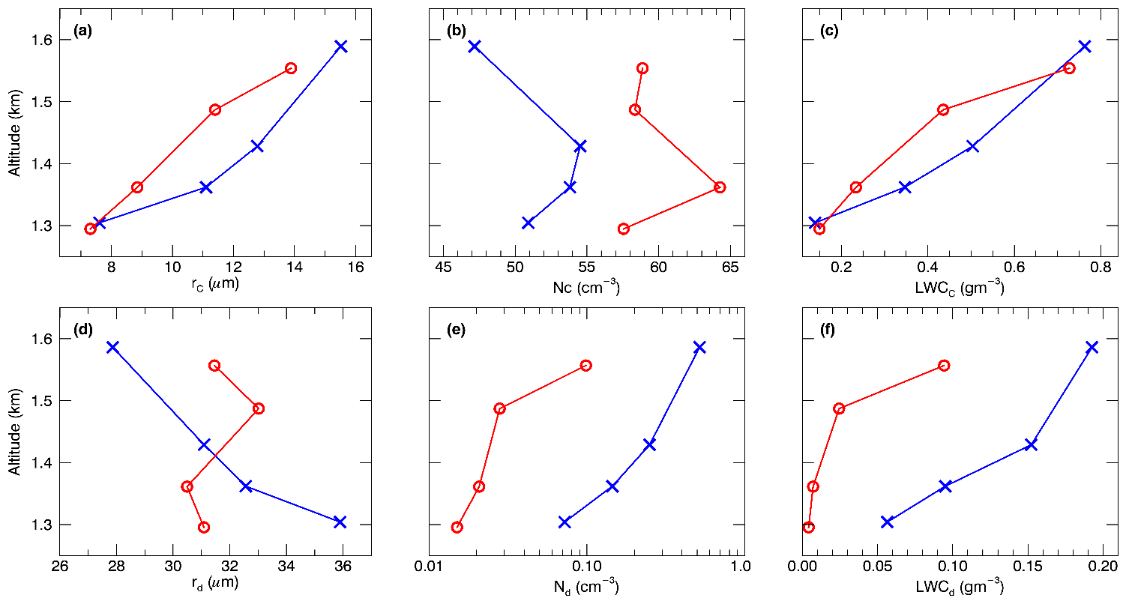

Figure 7. Same as Fig. 6, except for the mean values calculated from the 1 Hz aircraft in situ measurements along the horizontal legs shown in Fig. 1d on January 25.

https://doi.org/10.5194/acp-2020-817
Preprint. Discussion started: 25 August 2020

Atmospheric Chemistry and Physics
Open Access
EGU
Discussions

584

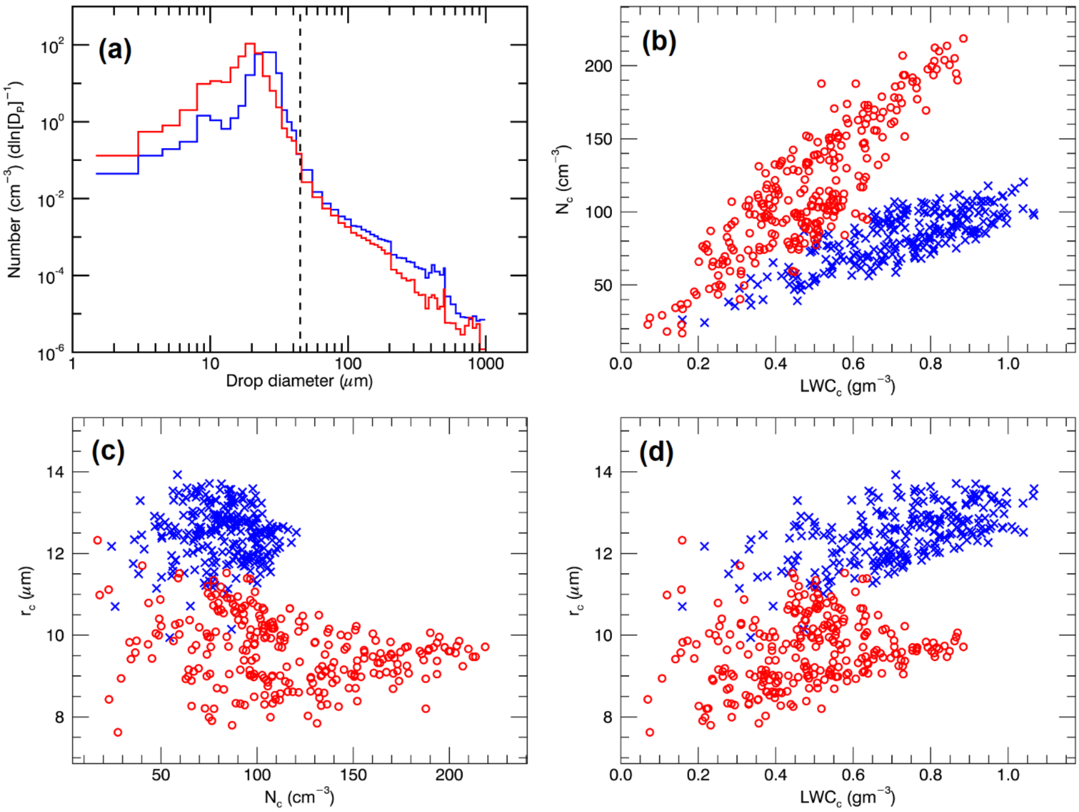

585

586

587 **Figure 8.** (a) Mean droplet size distribution (DSD) computed by averaging all 1 Hz in-situ measurements made for the horizontal legs at approximately 850 m altitude in the along-wind (blue) and cross-wind (red) directions on July 18. Approximate time range 10.0 to 10.15 UTC (refer to Fig. 1b). Vertical dashed line at drop diameter of 45 µm indicates the division between cloud-sized and drizzle-sized drops. The remaining panels are scatterplots of (b) cloud-droplet effective radius (r_c) vs. cloud-droplet number concentration (N_c), (c) N_c vs. cloud liquid water content (LWC_c) and (d) r_c vs. LWC_c derived from the 1 Hz in situ measurements taken along the 850 m horizontal legs.

595

https://doi.org/10.5194/acp-2020-817
Preprint. Discussion started: 25 August 2020

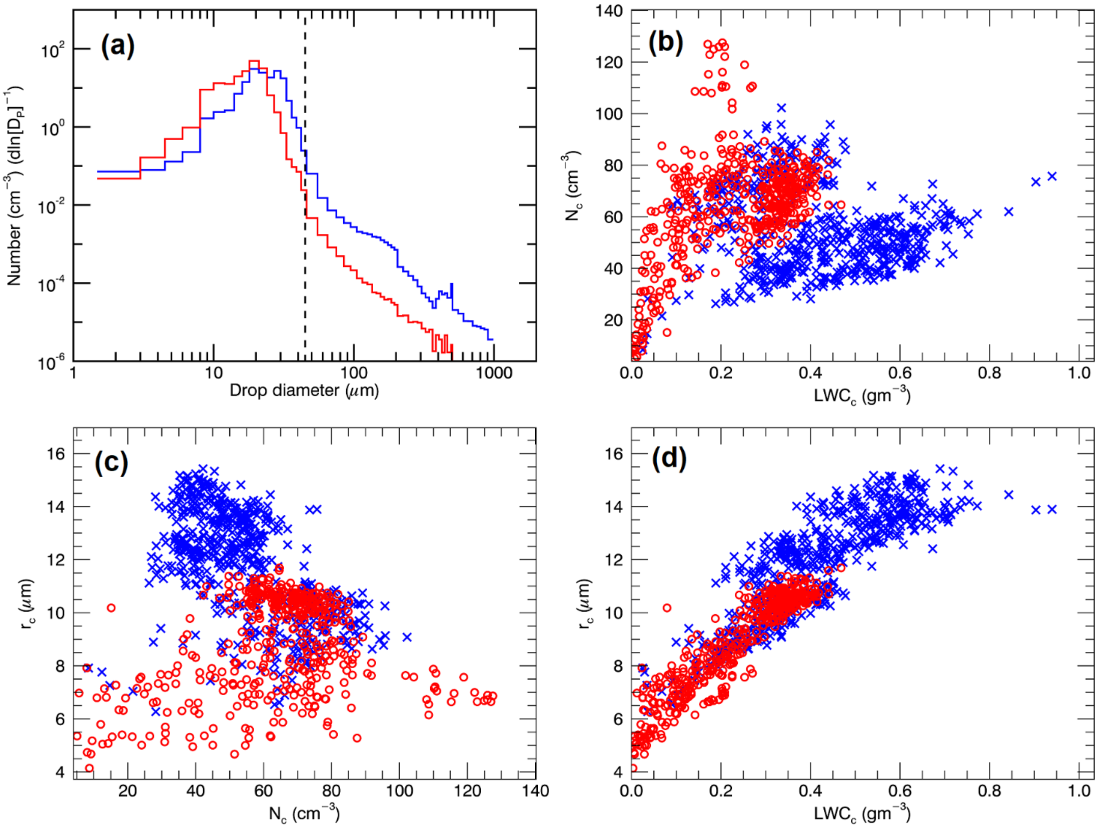

Figure 9. Same as Fig. 8, except for the in-situ measurements taken on January 25 when sampling the four horizontal legs in the middle altitude. Approximate time range is 11.95 to 12.35 UTC (refer to Fig. 1d).

https://doi.org/10.5194/acp-2020-817
Preprint. Discussion started: 25 August 2020

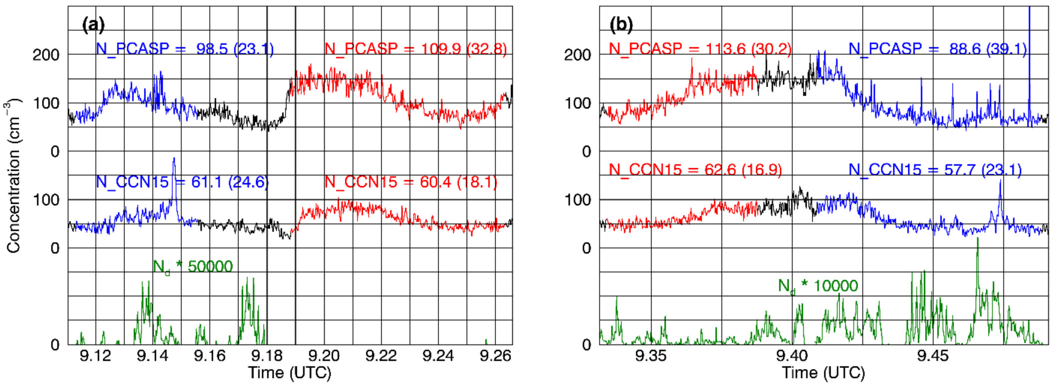

Figure 10. Observations of aerosol number concentration from the PCASP instrument and CCN at 0.15% supersaturation from the CCN counter on July 18 for horizontal legs (a) just above the ocean surface at 50 m altitude and (b) just below cloud base at 440 m altitude. Blue indicates the along-wind leg portion and red the cross-wind leg portion. Numbers show the mean and standard deviation for all 1 Hz in-situ measurements along each leg. Lower green lines are the observed drizzle drop concentrations scaled by factors of 50000 and 10000, respectively.

https://doi.org/10.5194/acp-2020-817
Preprint. Discussion started: 25 August 2020

Atmospheric Chemistry and Physics
Discussions

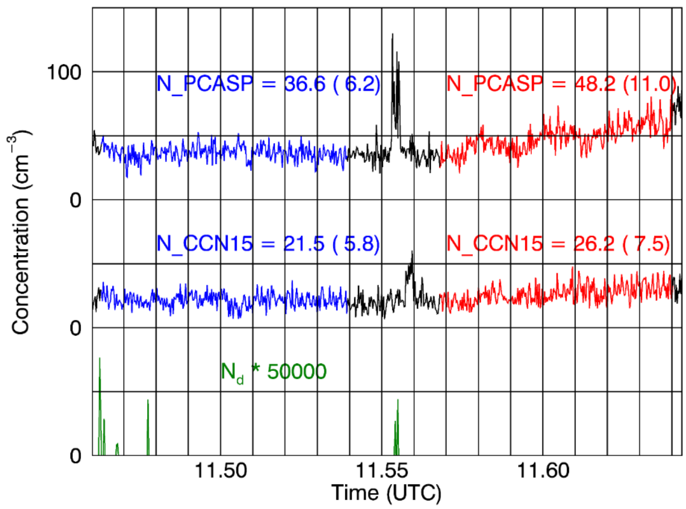

Figure 11. Same as Fig. 10, except for the in-situ measurements made at approximately 30 m above the ocean surface on January 25.

https://doi.org/10.5194/acp-2020-817
Preprint. Discussion started: 25 August 2020

Atmospheric Chemistry and Physics
Discussions

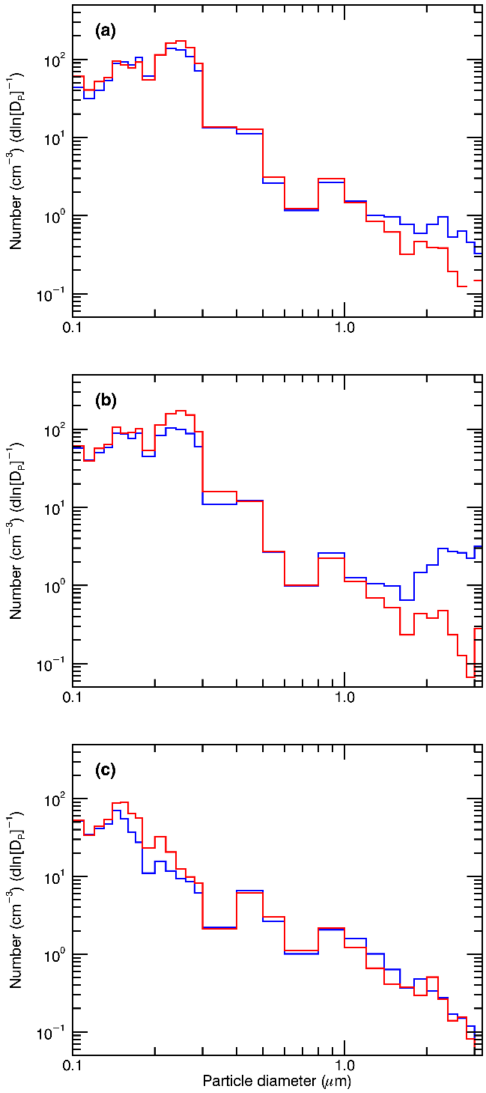

Figure 12. Mean aerosol size distribution computed by averaging all 1 Hz in-situ measurements of the size distribution from the PCASP instrument made along horizontal legs (a) on July 18 just above the ocean surface, (b) on July 18 just below cloud base, and (c) on January 25 just above the ocean surface. Blue indicates the along-wind leg portion and red the cross-wind leg portion.

https://doi.org/10.5194/acp-2020-817
Preprint. Discussion started: 25 August 2020

Atmospheric Chemistry and Physics
Discussions

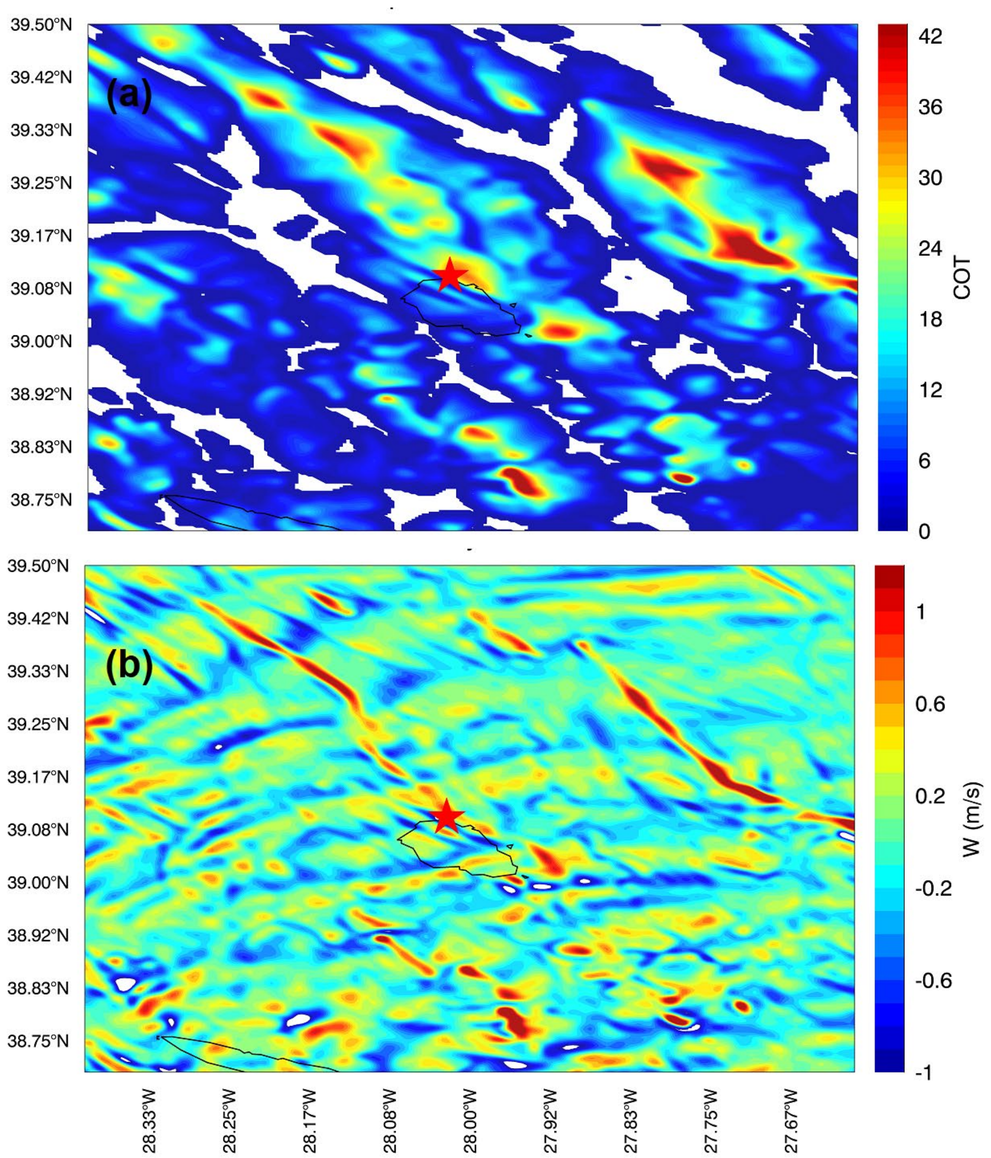

Figure 13. WRF simulation of (a) cloud optical thickness (COT) and (b) vertical velocity (w) at 848 m at 10:00 UTC over the inner domain of the model run. Red star indicates ARM radar facility. The black box in Fig. 3a outlines the WRF inner domain relative to the satellite imagery.